

Journal of Advanced Concrete Technology

Research and development of infrastructure diagnostic robot system (ALP) for detailed inspection of concrete structures at elevated heights

--Manuscript Draft--

Manuscript Number:	
Article Type:	Scientific Paper
Full Title:	Research and development of infrastructure diagnostic robot system (ALP) for detailed inspection of concrete structures at elevated heights
Abstract:	<p>This paper describes R&D of an inspection diagnostic system that applies robot technology to the detailed inspection of infrastructure such as concrete walls in high places. ALP uses a vacuum suction pad improved by testing on real structures as a moving mechanism. ALP is also fitted with a measurement system that consists of a high-resolution camera, an electromagnetic wave radar, and a hammering sound diagnostic device. The result is a highly capable self-propelling inspection system that can carry out detailed inspections of infrastructure in difficult-to-access locations such as high places.</p>
First Author:	Junichiro Noima, Ph.D.
Order of Authors:	Junichiro Noima, Ph.D.

Research and development of infrastructure diagnostic robot system (ALP) for detailed inspection of concrete structures at elevated heights

Junichiro Nojima (Manager of civil Engineering Dept., PhD, J-POWER DESIGN (JPD), Kanagawa, Japan), Toshiaki Mizobuchi (Professor, PhD, Hosei University, Tokyo, Japan), Kenji Hayashi (President of robot production company Stella Rtec Inc., Japan)

Abstract

This paper describes R&D of an inspection diagnostic system that applies robot technology to the detailed inspection of infrastructure such as concrete walls in high places. ALP uses a vacuum suction pad improved by testing on real structures as a moving mechanism. ALP is also fitted with a measurement system that consists of a high-resolution camera, an electromagnetic wave radar, and a hammering sound diagnostic device. The result is a highly capable self-propelling inspection system that can carry out detailed inspections of infrastructure in difficult-to-access locations such as high places.

1. Introduction

Infrastructure maintenance and management in Japan is a challenge owing to the rapid aging of the infrastructure that was mass produced during Japan' period of high economic growth and the shortage of skilled personnel. On the other hand, wholesale restoration of Japan's enormous social capital stock would not necessarily be most efficient and a more calibrated approach would work better. Hence, the assessment of the existing infrastructure is required to design optimal measures, yet superficial inspection based on simple visual inspection would fall short of providing the needed data. Accurate judgment of the causes of deterioration and whether it is of a progressive nature is required to determine the necessity of measures.

Use of non-destructive inspection for the detailed inspection of concrete structures has merits such as eliminating human error arising from differences among inspectors and revealing conditions inside concrete not detectable from external visual inspection alone. Use of the electromagnetic wave inspection method among the various nondestructive inspection methods allows measurement of cover concrete and thereby accurate judgment of whether repair during the service period is called for to remedy progressive deterioration. Further, by applying the chloride ion content determination technique using electromagnetic wave radar* developed by the authors, it is possible to determine the chloride ion content at the location of rebar, allowing prediction of latent stage deterioration from chloride attack.

However, in the case of structures in high places, scaffolds or the like are required for

human access, making detailed inspection more difficult. In recent years, the use of UAVs for infrastructure inspection has been increasing. However, detailed inspection such as described above necessitates bringing measuring equipment of a certain weight in stable contact with the wall surface, and considering the counterforce that must be applied to the wall surface to establish sufficiently stable contact with the structure, the use of UAVs is problematic. Therefore, we focused on vacuum suction pads and decided to develop an infrastructure diagnostic robot system called ALP. ALP is an abbreviation of the word "alpinist," and as such it carries the implied meaning of achieving the goal of executing detailed inspections even in difficult conditions such as high elevations (Nojima *et al.* 2018). Current wall-climbing robots from around the world are listed in Table 1. ALP was developed with the goal of achieving an apparatus capable of self-propelling up and down and left and right while stably adsorbed on a wall while equipped with various measuring devices.

2. Moving mechanism

2.1 Suction units

2.1.1 Suction unit mechanism (Figures 1, 2)

ALP has five suction units, three on the upper side and two on the lower side of ALP.

All suction units consist of the same suction/travel mechanism, and only the control firmware in each suction unit's microprocessor differs. Besides a microprocessor, each suction unit has also an adsorption unit equipped with a vacuum pump and a vacuum seal for secure adsorption on walls. The placement of the suction units on ALP is flexible as they can be mounted where desired on the ALP frame.

Each suction unit has an absorption unit mechanism that can move left and right, up and down, and extend and retract perpendicularly to the wall surface so as to achieve a good fit of the adsorption unit and its vacuum seal against the surface. Each suction unit is controlled independently with its own suction unit microprocessor, and the suction unit microprocessors are controlled by a main microprocessor via CAN interface.

2.1.2 Adsorption Power (Figure 3)

ALP can adsorb to rough and irregular wall surfaces such as weathered concrete and tiled surfaces with shallow joints with little air leakage.

The adsorption power of the adsorption unit is very strong. The adsorption power is calculated simply by $\pi \times R \times R \times V_{cur} / V_{abs}$,

where $\pi = \text{Pi}$; $R = \text{radius of the pad seal (cm)}$, $V_{cur} = \text{current vacuum value in the pad's vacuum chamber (kPa)}$, and $V_{abs} = \text{absolute vacuum value (kPa)}$.

For example, when the pad seal diameter is 16 cm and the vacuum value is -75 kPa in the pad's vacuum chamber, the calculated adsorption power is about 150 kg.

This value is the adsorption force in the direction perpendicular to a smooth wall surface. In actual practice, the adsorption power changes dynamically according to conditions such as vacuum leakage due to suboptimal contact surface conditions, rotational moment in the

downward direction of the suction pad under gravity, shifting loads on the suction pads due to slipping, movement of ALP, and movement of the center of gravity caused by movement of the measuring devices mounted on ALP.

2.1.3 Structure of ALP's adsorption unit seal

To maintain adsorption power, the adsorption unit seal is sophisticatedly designed to adapt to wall surfaces. The adsorption unit seal that contacts the wall surface is a cylindrical shape with a trumpet shaped edge made of silicone. The adsorption unit seal is over 10 mm high, which allows it cope with irregularities up to about 5 mm high and weathered concrete walls.

However, the surface layer of existing concrete structures tends to deteriorate under the influence of leaching and drying in places where it is exposed to rain, developing higher air permeability compared with parts that are shielded from rain (Torii *et al.* 1994). Experiments carried out on concrete walls with high air permeability in the surface layer revealed that it is not possible to achieve a stable vacuum state only with an adsorption unit seal.

On the other hand, the torrent method (Torrent 1994) is available as a surface layer quality test method. To eliminate the influence of air permeability of the surface layer of concrete, the torrent method employs a two-chamber vacuum cell. Taking inspiration from this method, the vacuum suction pads used by ALP were designed to achieve a stable vacuum state even on sub-optimum surfaces such as existing concrete whose surface quality has deteriorated by placing cushioning material around the sealing material so as to extend the air permeation path. (Figure 4)

The seal patent application number is Japanese Patent Application No. 2013-216032, the anti-gravity mechanism patent application number is Japanese Patent Application Nos. ongu 2017-002965 and 2018-002441, and the unit style robot configuration patent application number is Japanese Patent Application No. 2015-234253.

2.1.4 Related product (Figure 5)

As a related product, we also developed the Universal Gondola Stabilizer (UGS) based on ALP's suction pad architecture.

Gondolas are used for traveling up and down high-rise buildings. Since they are suspended from the rooftop by cables only, they are subject to shaking by work reaction force, strong winds, and the like. Thus gondola work crews must contend with the risk of falling and reduced work efficiency caused by gondola shaking.

In remedy these problems, we developed the UGS system, which constantly adsorbs to the walls of buildings even while ascending and descending, thereby eliminating gondola shaking.

The UGS system can easily be mounted to and removed from existing gondolas.

2.2 Moving mechanism of ALP adsorption unit

2.2.1 Left/right movement mechanism of adsorption unit (Figure 6)

The adsorption unit can move left and right to the desired position inside the suction unit frame. This movement is made possible by two belts provided above and below the suction unit and fixed to the adsorption unit, and that can be rotated clockwise and counterclockwise. The rotation of the belts is controlled by a microprocessor on the adsorption unit that controls a system consisting of belts, pulleys, a servomotor, and an encoder. The microprocessor on the adsorption unit can be communicated with and controlled by ALP's main microprocessor via the CAN interface.

2.2.2 U/down movement mechanism (Figure 6)

Similarly to the left/right movement mechanism described above, the adsorption unit can also move up and down to the desired position inside the suction unit frame. Movement is made possible by rotating clockwise or counterclockwise two belts provided on the left and right sides of the suction unit and fixed to the adsorption unit. The rotation of these belts is controlled by a microprocessor mounted on the adsorption unit and a mechanism that includes belts, pulleys, a servomotor, and an encoder. The microprocessor on the adsorption unit is communicated with and controlled by ALP's main microprocessor via the CAN interface.

2.2.3 Adsorption unit extension/retraction mechanism (Figure 7)

The adsorption unit can also extend toward and retract from the wall surface. This is done by extending or retracting the suction seal part of the adsorption unit facing the wall by turning the servomotor ball screw provided on the adsorption unit. Extension is done by extending the suction seal at the extremity of the adsorption unit that faces the wall in the direction of the target wall surface. When the suction seal contacts the surface, the suction seal part stops extending and vacuum suction is performed, making the suction seal part adhere to the wall surface and fixing the adsorption unit to the target wall surface.

2.2.4 ALP climbing motion on wall surface (Figures 6, 7)

As described above, the adsorption unit can move right/left and up/down in the suction unit. Further, the suction seal part of the adsorption unit can perpendicularly extend toward and retract from the wall surface.

If the suction unit moves downward while the suction seal part is adsorbed to the wall surface, the suction unit moves upward on the wall surface.

If the adsorption unit moves downward while the suction seal part is not adsorbed to the wall surface, the suction unit does not move and only the adsorption unit moves downward. In this way, depending on whether or not the suction seal part is adsorbed to the wall surface, the suction unit will either ascend the wall surface or not.

As described above, as the various suction units repeatedly perform this operation, ALP is able to climb up the wall while securely clinging to its surface. The operation of the suction units and the adsorption units is made possible by controlling the suction units and the main microprocessor.

2.3 ALP control method, power supply and safety

2.3.1 ALP remote control (Figures 8, 9)

ALP can be operated by remote control via wireless or via a composite cable combining an optical fiber cable, a power cable, and a safety suspension cable. The main microprocessor controlling the entire ALP system can also be controlled from a remote PC via wireless, and it is also possible to connect a PC mounted on ALP to a remote PC by optical fiber cable for communication and control purposes.

In the case of control via optical fiber cable, very fast communication speed is achieved, allowing not only control of ALP, but also control of the measurement tools and acquisition by the remote PC of the enormous amounts of measurement data they generate, including photographic data.

Use of a long-distance composite cable allows not only the acquisition of huge amounts of measurement data, but also power supply and even safe suspension.

2.3.2 ALP power consumption (Figure 9)

ALP uses 100 VAC and consumes less than 3 A.

In the case of wireless operation, a separate power supply cable must be provided, and in the case of operation by composite cable, power supply is provided by the power supply cable incorporated in the composite cable.

2.3.3 Safety (Figure 10)

ALP normally climbs walls on its own.

ALP is designed to use commercial power supplies.

If the commercial power supply used by ALP is momentarily interrupted, the UPS (Figure 9) will supply electric power to ALP automatically until commercial power supply resumes.

While ALP is designed to climb walls on its own, if it were to drop due to failure, ALP's fall will be arrested by safety suspension cables or the composite cable, which incorporates a safety suspension cable (Figure 10).

3. Measurement mechanism

The measuring mechanism can move the measuring devices by 1 m in the horizontal direction and stably press them against the wall surface for precise measurement.

As shown in Figure 11, the measurement mechanism is equipped with a high-resolution camera, a hammering device, and an electromagnetic wave radar. The high-resolution camera has a resolution of 51.5 million pixels that allows it to discern cracks just 0.2 mm in width. The hammering device uses a solenoid magnet to strike the wall surface, picking up the reflected sound with a microphone to detect scaling of concrete. The electromagnetic wave radar can estimate the position of the rebar and the depth of cover concrete. Moreover, it allows

estimation of the chloride content in the cover concrete by using the attenuation rate of the electromagnetic waves reflected from rebar.

3.1 Image capture system using high-resolution camera

Close visual inspection is an inspection action that consists in approaching the object to be inspected and visually checking for deterioration such as cracks and spalling, recording observations in the form of sketches. In the case of ALP, a robot approaches the surveyed object on behalf of a person, so a camera must be mounted to perform close visual inspection. For cracks, auxiliary instruments such as a crack scale are usually required for measurement and recording of the width and length of cracks.

For the purpose of supporting close visual inspection by ALP, experiments using imaging with a high-resolution digital camera and 3D modeling were carried out. The camera used was a 51.5 million pixel camera, shown in Figure 12, and a test shooting platform was also employed, with the aim of capturing cracks with a width as small as 0.2 mm, equivalent to a 4-pixel span. Further, since the 3D modeling is done using a precision photogrammetry technique, the camera position was moved using a slider mechanism so that to obtain an overlap ratio between captured images of 60% or more, and a total of seventy pictures covering a surface area of 1 m² were taken.

The acquired image data were combined to create a 3D model using Structure from Motion (SfM) (Snavely *et al.* 2006,2007) (see Figure 13), and the accuracy of the constructed 3D model was verified by distance measurement with a TIN mesh (see Figure 14). Beforehand, a qualified concrete diagnostician confirmed with a crack scale crack widths of 0.1 mm and 0.2 mm, and the crack widths were measured at the same locations on the 3D model. As a result, the measured value was found to be 0.131 mm in the 0.1 mm crack range, and 0.210 mm in the 0.2 mm crack range. From the above, it was confirmed that a 3D model allowing detection of cracks of width as small as 0.1 mm can be constructed by using a high-resolution digital camera from the shooting position of ALP.

3.2 Electromagnetic wave radar

To detect the position of rebar in the concrete and the thickness of the cover concrete, an electromagnetic wave radar was mounted on ALP. Elsewhere, the authors have reported on the possibility of determining the chloride ion content of concrete through the use of electromagnetic waves (Mizobuchi *et al.* 2003-2008). Furthermore, studies by Kurumisawa *et al.* have shown the possibility of verifying differences in chloride ion content using the rebar reflected waveform of electromagnetic waves in specimen experiments using the finite difference time domain method (FDTD). This technology is used to determine chloride ion content by non-destructive inspection of structures near the coast and roads where snow-melting agents are used. Compared with the conventional method combining core sampling and potentiometric titration, this technology excels both in terms of the amount of

acquired data and implementation cost.

Given that the electromagnetic wave radar is mounted on ALP, it should be lightweight and radio controllable, and thus an electromagnetic wave radar of the specifications listed in Table 2 was adopted instead of the equipment that was used for determination of chloride ion content by electromagnetic wave radar.

3.2.1 Principle of technology for determination of chloride ion content in concrete by electromagnetic waves (SAE) (Nojima *et al.* 2011-2016)

When the electromagnetic wave is sinusoidally oscillating at a single angular frequency ω , assuming it as a one-dimensional wave equation, equations (1) and (2) are derived using the vector wave equation.

$$\nabla^2 E + k^2 E = 0 \quad (1)$$

$$\nabla^2 H + k^2 H = 0 \quad (2)$$

$$(k^2 = \omega^2 \varepsilon \mu - j \omega \mu \sigma)$$

where E is the electric field (V/m) and H is the magnetic field (A/m). where E is the electric field (V/m) and H is the magnetic field (A/m), k is the propagation constant, and σ is the conductivity (S/m).

Usually, when propagation constant k is a complex number, it can be divided into a real part and an imaginary part,

$$k = \sqrt{\omega^2 \varepsilon \mu - j \omega \mu \sigma} = \beta - j \alpha \quad (\alpha > 0, \beta > 0) \quad (3)$$

with α and β as follows.

$$\alpha = \omega \sqrt{\frac{\varepsilon \mu}{2}} \left\{ \sqrt{1 + \frac{\sigma^2}{\omega^2 \varepsilon^2}} - 1 \right\}^{1/2} \quad (4)$$

$$\beta = \omega \sqrt{\frac{\varepsilon \mu}{2}} \left\{ \sqrt{1 + \frac{\sigma^2}{\omega^2 \varepsilon^2}} + 1 \right\}^{1/2} \quad (5)$$

When a plane wave with polarization in the x direction propagates in the z direction, the following equation is obtained when expressed using terms α and β .

$$E = \hat{x} E_0 \exp(-jkz) = \hat{x} E_0 \exp(-\alpha z - j\beta z) \quad (6)$$

The real part β of transmission constant k in equation (3) is the phase constant, and the imaginary part α is the attenuation constant, indicating that as the electromagnetic wave propagates, its

gradually attenuates. In other words, the magnitude of the electric field $|E|$ is expressed by

the attenuation function shown in equation (7), and as the electromagnetic wave travels in the z direction, it attenuates. Thus, the higher the value of attenuation constant α , the shorter the propagation distance at which the electromagnetic wave attenuates.

$$|E| = |E_0| \exp(-\alpha z) \quad (7)$$

Chloride attack occurs when chloride ions from airborne salt and snow-melting agents penetrate concrete and diffuse in the concrete pore solution, speeding up the progress of corrosion of rebar in concrete. The phenomenon of the conductivity of sea water being higher than that of ultra pure water and tap water is due to the fact that strong electrolytes such as NaCl dissolve in water, forming ions that play the same role as free electrons in metals, thereby increasing the electrical conductivity of the aqueous solution. The same phenomenon occurs when chloride ions are present in the pore solution of concrete, causing conductivity σ to rise and resulting in a higher attenuation constant of electromagnetic waves, per equation (7).

In view of the above, the authors focused on the following in earlier studies.

1) Development of a theory of electromagnetic wave attenuation in the presence of chloride ions in concrete

2) Determination of the degree of influence of the major electromagnetic wave attenuation factors of "chloride ion content," "electromagnetic wave propagation distance," "moisture content," and "temperature" by varying these factors in concrete specimens.

3) Development of electromagnetic wave attenuation simulation from the attenuation characteristics of electromagnetic waves in concrete obtained from electromagnetic wave attenuation theory and specimen experiments (hereafter, SAE (Simulation of Attenuation Electromagnetic waves), Equation (8))

4) Determination of electromagnetic wave attenuation and chloride ion content in concrete specimens and actual structures under various conditions with SAE

The amplitude value (Figure 16) as used here indicates the ratio of the reflected energy from rebar to the input wave, which is similar to electric field magnitude $|E|$ in Equation (7). Figure 17 shows the method of amplitude value acquisition by electromagnetic wave radar in SAE.

3.2.2 Study toward assessment of actual structures

With a view to applying SAE to the assessment of actual structures with ALP, the following items were investigated.

[1] Investigation of stability of amplitude value of electromagnetic wave radar

[2] Influence of surface roughness on irregular surface reflection of electromagnetic waves

[1] Investigation of stability of amplitude value of electromagnetic wave radar

The amplitude value applied in the present study was confirmed in past research to change as the temperature rises when the antenna circuit inside the equipment is energized, and to stabilize as the temperature becomes constant. Since the electromagnetic wave radar to be mounted on ALP differed from the electromagnetic wave radar used in past research, the optimum stabilization wait time was determined using specimens.

For the chloride ion content of 0 kg/m^3 and cover thickness of 50 mm, the measured value was found to come within $\pm 5\%$ of the value measured at 1 hour from measurement start after the lapse of 19 minutes. For the chloride ion content of 2.4 kg/m^3 and cover thickness of 100 mm, the value came within $\pm 5\%$ after the lapse of 17 minutes. Based on the above results, it was determined that the measured value can be considered to become stable at about 20 minutes from the start of measurement, since the cover thickness and chloride ion content of concrete are not known when performing measurement of actual structures. (Figure 18)

[2] Investigation of the influence of surface roughness on irregular surface reflection of electromagnetic waves

Indoor test specimens with varying surface roughness were fabricated and used to examine the influence of surface roughness on irregular surface reflection of electromagnetic waves. In addition, the concrete surface of an actual structure was measured with a 3D scanner and the obtained data was processed for data analysis. (Figure 19)

As a result, it was confirmed that when the surface roughness is large, incident waves are scattered by the concrete surface and the reflection amplitude value from rebars is smaller compared with concrete that has a smoother surface. (Figure 20)

Figure 21 shows the results of chloride ion content estimation carried out on a concrete structure by the sea. The salinity maps shown on the middle and bottom level in this figure indicate differences in estimated values based on the magnitude of correction done in view of the representative surface roughness of each block indicated by a red frame as measured by 3D scan. This figure confirms that the amount of penetration by chloride ions in the two rightmost red frames is small as the result of surface roughness correction, and that the concrete structure is sound. Further, the sea side of the two rightmost red frames is a ship anchoring location, and as such it is protected from the influence of airborne salt.

The result of collecting cores from each red frame and calculating the chloride ion content by potentiometric titration, and the chloride ion content determined by electromagnetic wave SAE are shown in Figure 22. This figure confirms that through appropriate assessment of the influence of surface roughness, values that closely approximate actual measurement values can be obtained.

Since ALP is not equipped with a 3D scan device, the influence of surface roughness will likely be assessed through the use of precision 3D models obtained from SfM.

3.3 Hammering device

The hammering device mounted on ALP uses a compact solenoid magnet designed specifically for automatic striking to achieve hammering action, and the resulting reflected sound is recorded with a condenser microphone and used to detect scaling and other flaws. Generally, bending vibration theory is applied to the reflected sound produced by scaling parts. As shown in Figure 23 (Utagawa *et al.* 2013), bending vibration can be used to detect flaws due to the fact that the thinner a member is, the larger the bending vibration it produces. Somewhat similarly for the hammering device of ALP, the characteristic of scaling parts that, compared with the initial wave of the impact sound (P1), the reflected sound (P2) is of greater amplitude, whereas the opposite holds true for the sound parts of concrete, is used to detect scaling. (Figure 24)

3.3.1 Improvement of exploration depth of hammering system

In the conventional type created during the early development period, sufficient hammering energy was not achieved due to the short stroke of the hammer part, the small hammering energy, and voltage drop of the connecting cable. Therefore, a new hammering device improving all these points was created. As a specific countermeasure against the voltage drop, the diameter of the cable was changed to about twice the previous thickness to increase the voltage applied to the solenoid and to prevent the voltage drop of the connecting cable. The old and the improved hammering devices are shown in Figure 25 and Figure 26.

Shape: ϕ 45 mm \times 106 mm (excluding protrusions) Sound recording: Waterproof condenser microphone Hammer: ϕ 10 mm cylindrical stainless steel hammer Hammer stroke of 9 mm, hammering cycle fixed to 2 Hz
--

3.3.2 Specimen test

To verify the striking element improvement effect, specimens with a simulated void 400 mm wide, 100 mm long, and 100 mm thick were prepared, and the performance comparison of the conventional type and the improved type was conducted.

The area under each of the numbers lined up from the left side of the specimen shown in Figure 27 corresponds to the hammering points. The area under [2] has a simulated void 10 mm below the concrete surface that measures 50 mm \times 50 mm \times 10 mm (width \times length \times thickness), the areas under [4] has a simulated void 30 mm below the concrete surface that

measures 50 mm × 50 mm × 10 mm, and the area under [2] has a simulated void 50 mm below the concrete surface that measures 50 mm × 50 mm × 10 mm. The other areas under [1], [3], [5], and [7] are sound areas free of flaws.

The test conditions in this evaluation were the following four cases. (Figures 28, 29)

- Case 1: 9 V driven conventional type
- Case 2: 12 V driven conventional type
- Case 3: 9 V driven improved type
- Case 4: 12 V driven improved type

The test results of each case were as follows.

[Case 1: 9 V driven conventional type]

The measurement results show reliable detection of the 10 mm deep void, but unreliable detection of the 30 mm deep and 50 mm deep cavities.

[Case 2: 12 V driven conventional type]

The measurement results show reliable detection of the 10 mm deep void, but unreliable detection of the 30 mm deep and 50 mm deep cavities. This is presumably due to the voltage drop of the cable and still insufficient striking force despite the increased drive voltage.

[Case 3: 9 V driven improved type]

The measurement results show reliable detection of the 10 mm deep void, as well as the possibility of detecting cavities even at depths of 30 mm and 50 mm.

[Case 4: 12 V driven improved type]

The measurement results show reliable detection of the 10 mm and 30 mm deep cavities. The 50 mm deep void too gave a discernible waveform, showing the possibility of detecting cavities even at this depth.

3.3.2 Performance verification on actual structures

Performance verification of the hammering device was carried out at the N2U-BRIDGE (New Bridge) facility (Figure 30) for bridge inspection technology study and research at Nagoya University. Performance verification was carried out at the following four places.

- [1] Simulated void specimen depth: 30 mm, size: 500 mm × 500 mm
- [2] Simulated void specimen depth: 80 mm, size: 600 mm × 350 mm
- [3] Cracked test specimen
- [4] Former Shibue River—cracked part on back of removed deck slab

The results of the performance verification are shown below.

[1] Simulated void specimen depth: 30 mm, size: 500 mm × 500 mm (Figures 31, 32)

As the result of the performance verification, a clear difference between the hollow part and the sound part was confirmed. In the hollow part, the peak values of P1 and P2 are both large, clearly indicating a void detection waveform.

[2] Simulated void specimen depth: 80 mm, size: 600 mm × 350 mm (Figures 33, 34)

As the result of the performance verification, a clear difference between the hollow part and the sound part was confirmed. Regarding the detected waveform for the void at the depth of 80 mm, while in some locations the void could not be detected as such, at the center of the hollow portion, the waveform clearly shows the characteristics of a void, and clearly differs from the waveform obtained from the sound parts.

[3] Cracked specimen depth: 80 mm, size: 300 mm × 300 mm (Figures 35, 36)

The performance verification showed that the cracked part returned a waveform similar to that of the sound part, and that the wavelengths of both P1 and P2 both being long makes it difficult to distinguish between the sound part and the cracked part.

[4] Former Shibue River—cracked part on back of removed deck slab (Figures 37, 38)

The performance verification showed that delamination due to cracks can be detected quite clearly. While detection is possible also to some extent from P1 and P2, in scaling parts, P2 is clearly larger than P1. A clear difference could be seen between the waveforms obtained from sound parts surrounded by cracks or parts without severe delamination, and parts with severe delamination near cracks. Figure 38 shows a color-coded representation of the numerical values measured at the marked location showing delamination.

From the above, taking into consideration the results of the specimen test and the performance verification on actual structures, it was confirmed that the maximum void detection depth of the hammering device mounted on ALP is 50 mm or less.

4. Experimental results on actual structure

The ALP demonstration experiment was carried out on the side wall of the intake gate concrete pier of an arch type dam. Because the ALP is heavy, it was moved from the transport vehicle to the wall of the target using a lifter. Thereafter, ALP self-propelled along the wall and acquired accurate data by remote control. The power supplied to ALP was supplied by power cable from a small 0.9 kVA gas-cylinder-type generator. The acquired data was analysed over five hours to generate a three-dimensional model by SfM. Figure 39 shows the high-resolution three-dimensional model obtained as the result of fine inspection by ALP, and the data acquired by the hammering device and electromagnetic wave radar. The data shown in Figure 39, which covers an area of approximately 1 m², took approximately 2 hours to acquire, including ALP operation and measuring time.

4.1 Comparison with measurement by humans

Alongside measurement by ALP, measurement by humans was also conducted at the same locations, and the respective results were compared. The purpose of this comparison was to find out whether ALP can produce results comparable to those achieved by humans at inspection locations that humans are unable to access.

The results are summarized in Figure 40. As seen from Figure 40, in terms of precise 3D model by SfM and the results of the electromagnetic wave survey, there were slight differences between the data acquired by ALP and by humans, but only to a limited extent, and the data produced by ALP was confirmed to be suitable for practical use without any problem. This is due to the fact that the vacuum suction pads used by ALP provided stable adsorption even on concrete walls with unevenness. On the other hand, the hammering device was unable to achieve stable hammering against unevenness on walls. Going forward, it will be necessary to improve ALP's pressing mechanism or the solenoid driven striking element.

4.2 Utilization of acquired data as detailed inspection data

ALP is capable of close-up overlapping photographic capture with a high-resolution camera in high places with good stability. The acquired images can then be used to create a precise 3D model with SfM. Figures 41 and 42 show 3D models created from the image data acquired by ALP. ALP makes it possible to simultaneously obtain non-destructive inspection results from electromagnetic wave radar and hammering device, allowing judgment of factors and progress of deterioration even without engineers near the target structure. Further, ALP surveys are non-destructive inspection, allowing simultaneous inspection of the same location by two or more times. Moreover, for local inspection records using crack scales or the like, ALP's ability to create 3D models with local coordinates makes it possible to precisely judge the progress of deterioration. Based on the above, ALP can be said to produce valuable data that can be used to verify the deterioration of concrete with considerable precision.

On the other hand, ALP moves slowly compared with UAVs. Considering the time and costs involved in inspection, it would be desirable to first confirm deterioration locations from general imaging results obtained by UAV and then carry out detailed inspection by ALP in a specific range.

5. Conclusions

The results obtained by research and development of the ALP infrastructure diagnostic robot system capable of operating under difficult conditions such as high places are summarized below.

(1) A system to acquire data required for detailed inspection of concrete without direct access by people was created and tested.

(2) Vacuum suction pads that can stably adsorb onto uneven concrete walls were created.

(3) To further improve the judgment accuracy of engineers regarding flaws in concrete, multiple types of non-destructive inspection and precise 3D modeling allow detailed inspection.

On the other hand, as the whole ALP system has considerable weight and its moving speed is slow, it can take a lot of time to access target locations, and in some cases, obstacles may well prevent access altogether. Going forward, we expect various innovations and beneficial effects from synergies produced by combining the vacuum suction pads developed this time and other technologies.

Finally, This ALP practical development project was obtained by the subsidy of New Energy and Industrial Technology Development Organization (NEDO).

References-----

- Nojima, J., Mizobuchi, T., (2018). "Research and development of infrastructure diagnostic robot system (ALP) by concrete wall moving mechanism using vacuum suction pad." *Syner Crete'18*, 13, 135-146.
- Torii, K., Kawamura, M. and Ueda, S., (1994) "Over several 80 years deterioration of concrete situation", *Cement Science and concrete Technology*, No.48, pp.518-523. (in Japanese)
- R.J.Torrent, (1992), "A two-chamber vacuum cell for measuring the coefficient of permeability to air of the concrete cover on site", *Material and Structures*, 25, pp.358-365.
- Snavely, N., Seitz,S.M., and Szeliski,R., (2006), "Photo Tourism : Exploring image collections in 3D", *ACM Transactions on Graphics (Proceedings of SIGGRAPH 2006)*.
- Snavely, N., Seitz,S.M., and Szeliski,R., (2007) , "Modeling the World from Internet Photo Collections". *Int'l. J. Computer Vision*.
- Mizobuchi, T., Arai, J. and Suda, K., (2003), "Experimental Study on Measurement of Chloride Content using Electromagnetic Wave in Reinforced Concrete Structures", *Structural Faults and Repair-2003*, 241-248.
- Arai, J., Mizobuchi, T. and Suda, K., (2003), "Study on Measurement of Chloride Content using Electromagnetic Wave in Reinforced Concrete Structures", *Non-Destructive Testing in Civil Engineering*.
- Mizobuchi, T., Suda, K., Hayashi, D. and Yokozeki, K., (2005), "Experimental Study on Applicability of Measuring Method of Chloride Content using Electromagnetic Wave in Reinforced Concrete Structures" , *The 11th International Conference on Fracture*.
- Hayashi, D., Mizobuchi, T., Suda, K. and Yokozeki, K., (2005), "Experimental Study on Applicability of Measuring Method of Chloride Content using Electromagnetic Wave in Reinforced Concrete Structures" , *The Third US-Japan Symposium on Advancing Applications and Capabilities in NDE*.
- Mizobuchi, T., Yokozeki, K. and Ashizawa, R., (2006), "Applicability of Estimation of Chloride Content using Electromagnetic Wave in Reinforced Concrete Structures", *Structural Faults and Repair-2006*
- Mizobuchi, T., Yokozeki, K., Watanabe, K. , Hiraishi, M. and Ashizawa, R., (2007), "Monitoring System of Chloride Content in Cover concrete using Electromagnetic Wave and Impedance Method", *Proceedings of the 6th International Conference on Fracture Mechanics of Concrete and Concrete Structures*,1865-1876.
- Mizobuchi, T., Yokozeki, K., Watanabe, K. and Ashizawa, R., (2007), " Applicability of Estimation of Chloride Content using Electromagnetic Wave in coastal Reinforced Concrete Structures" , *Proceeding of the 5th International Conference on Concrete under Severe Conditions of Environment and Loading*, 499-512.
- Mizobuchi, T., Yokozeki, K., Watanabe, K. and Ashizawa, R., (2008), "Applicability of Estimation of Chloride Content in Cover concrete using Electromagnetic Wave and Impedance Method", *on Site Assessment of Concrete, Masonry and Timber*.

- Mizobuchi, T., Yokozeki, K., Watanabe, K. and Ashizawa, R., (2008), “Applicability of Estimation for Distribution of Chloride Content in Cover concrete using Electromagnetic Wave”, *Structural Faults and Repair-2008*.
- Nojima, J. and Mizobuchi, T., (2011), “Applicability of Electromagnetic Wave Method for Estimation of Chloride Content of Coastal Structures”, *Concrete Solutions-2011*.
- Nojima, J. and Mizobuchi, T., (2011), “Application of an Electromagnetic Method for Evaluation of Chlorine Distribution in Concrete”, *NDTMS-2011*.
- Mizobuchi, T. and Nojima, J., (2011), “Applicability of Estimation of Chloride Content in Cover concrete of Coastal Reinforced Concrete Structures using Electromagnetic Wave”, *NDTMS-2011*.
- Nojima, J., Ikeda, H., Mizobuchi, T., (2012) “Possibility of Estimation of Chloride Content in Concrete to Existing Structures Using Electromagnetic Wave”, *Structural Faults and Repair-2012*.
- Nojima, J., Ikeda, H., Uchida, M and Mizobuchi, T., (2013). ”Theoretical And Experimental Study On Estimation Of Chloride Content In Concrete Using Electromagnetic Wave”, *SPIE Smart Structures NDE 2013*
- Nojima, J., Uchida, M. and Mizobuchi, T., (2015). “Study on possibility of estimation of chloride content in coastal reinforced concrete structures using electromagnetic waves.” *ICCRRR 2015*.
- Nojima, J., Uchida, M., Arai, J. and Mizobuchi, T., (2015). “A Study on Estimation Method of Chloride Content in Concrete Using Electromagnetic Waveform.” *Proceedings of the Japan Concrete Institute*, Vol.37, No.1, 1675-1680. (in Japanese)
- Nojima, J., (2015). “Study on Accuracy Improvement and Practical Application for Estimation of Chloride Content in Concrete Structures Using Electromagnetic Wave Method.” *PhD Thesis*, Hosei University. (in Japanese)
- Nojima, J., Uchida, M., Arai, J and Mizobuchi, T., (2016). “Fundamental study on improvement of estimation accuracy of content of chloride ions in concrete using electromagnetic waves method.” *Journal of Japan Society of Civil Engineers E-2*, vol.72, No.2, 109-125. (in Japanese)
- Utagawa, N. and Misaki, N., (2013) “Diagnosis of tunnel lining concrete”, *Acoustical Society of Japan*, vol.69, No.3, 127-132. (in Japanese)

Figure & Table-----

Table 1 Wall-climbing robot

	ALP (Figure 1)	Vortex VRAM	ICM Climber	Wall Climbing Robot	Mecho-Gecko
Developer	Stella Rtec	Vortex HC LLC	ICM	SRI	UCLA
URL	http://www.stella-rtec.co.jp/	https://www.cnet.com/news/wall-climbing-robot-sucks-it-up	http://www.icm.c/c/	https://www.sri.com/sites/default/files/brochures/sri_wallclimbingrobots.pdf	http://www.ijmer.com/papers/Vol2_Issue6/CP2643474351.pdf
Adsorption method	Vacuum pump	Blower	Blower	Electrostatic	Van der Waals
Adsorption wall	Irregular surface <5-7 mm	Irregular surface <2-4 mm	Irregular surface <2-4 mm	Irregular surface	Irregular surface
Status	Commercialized	Commercialized	Commercialized	Academic purpose	Academic purpose
Payload	Heavy	Extremely light	Light	Extremely light	Extremely light
Climbing speed	Slow	Fast	Fast	Extremely slow	Extremely slow



Fig. 1 ALP

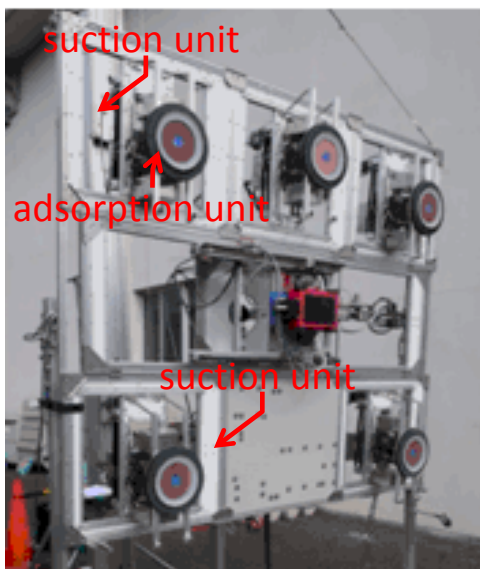


Fig. 2 ALP(suction side)

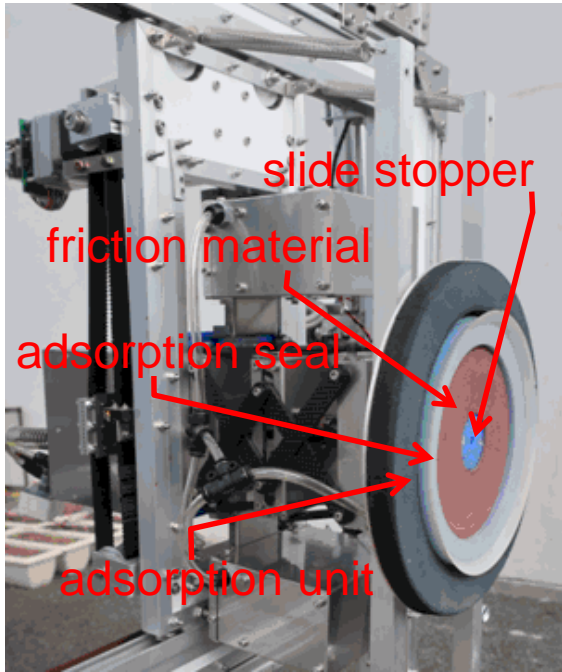


Fig.3 Adsorption unit



Fig.4 Adsorption target of vacuum suction pads



Fig.5 Universal Gondola Stabilizer

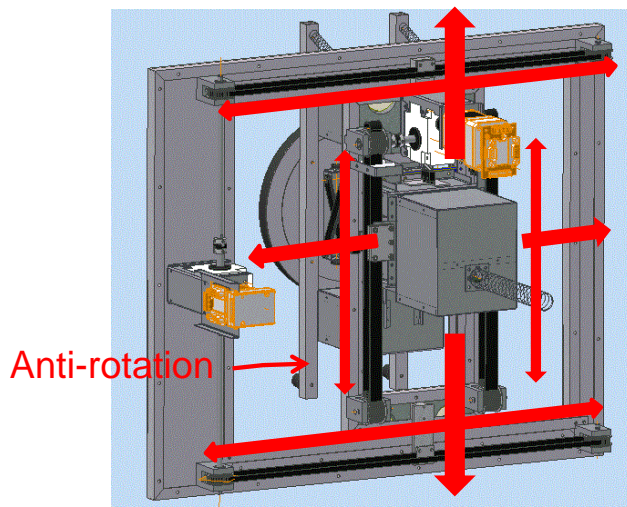


Fig.6 Suction/travel mechanism (1)

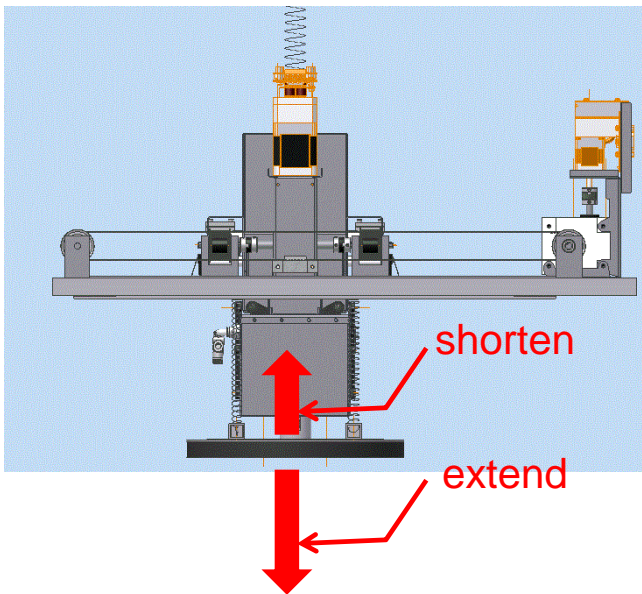


Fig.7 Suction/travel mechanism (2)

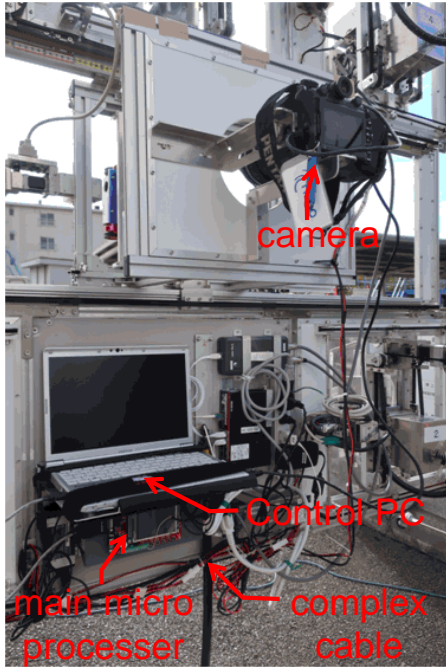


Fig.8 ALP remote control

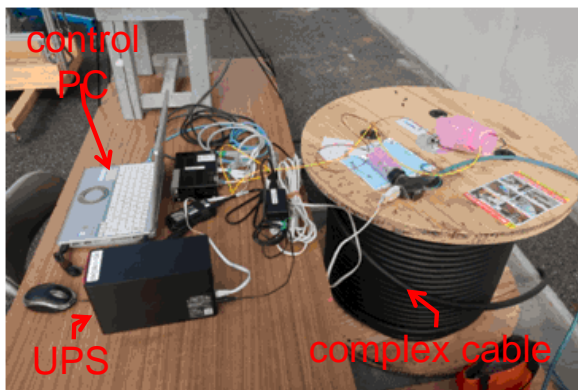


Fig.9 ALP power consumption



Fig.10 Safety

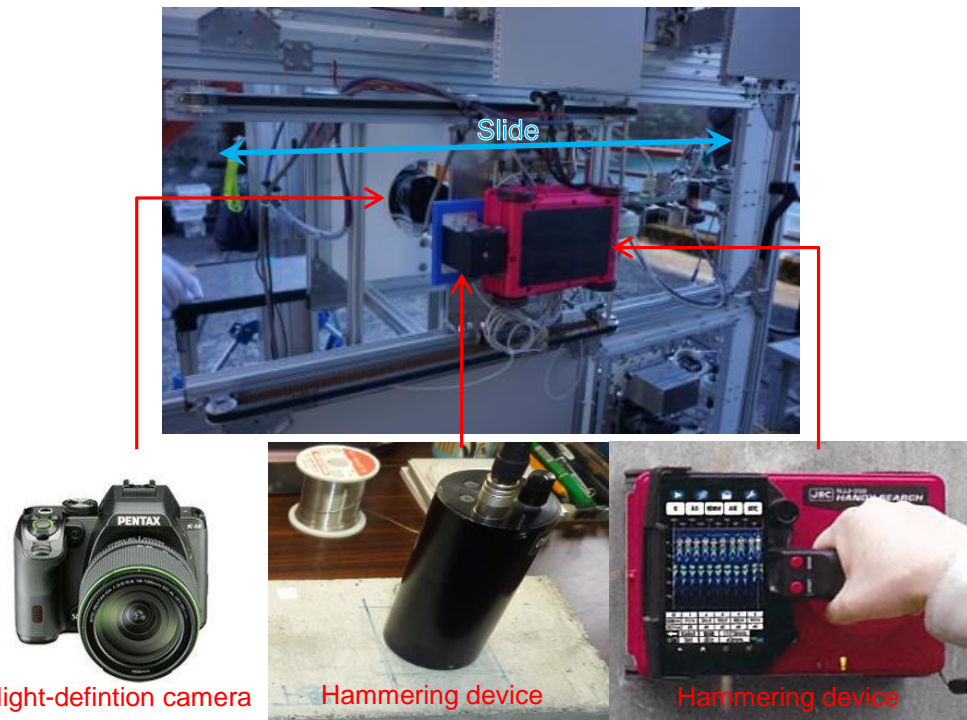


Fig. 11 ALP mounted measuring instruments

Shooting camera	PENTAX 645Z
Using lens	PENTAX 645Z-35mm
Shooting distance	48.4cm
Angle of view (a cut)	Approximately 40×30cm
Total pixels	8156×6192
ISO	200(Default)
Data capacity	JPG:1.94GB/70 pictures



Fig. 12 High-resolution digital camera

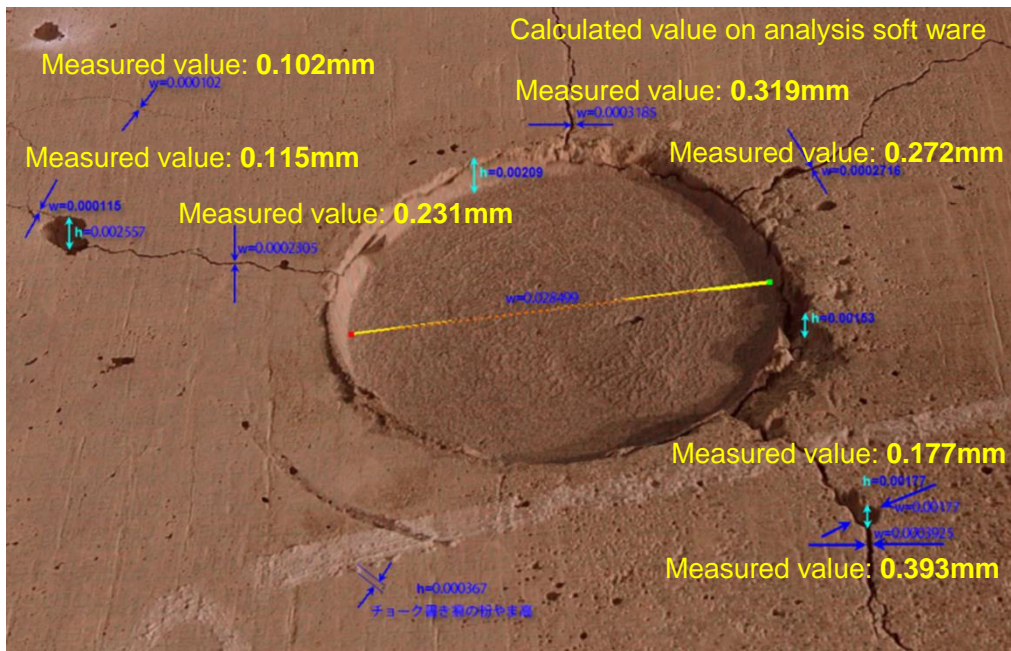


Fig. 13 Concrete wall surface (3D model)

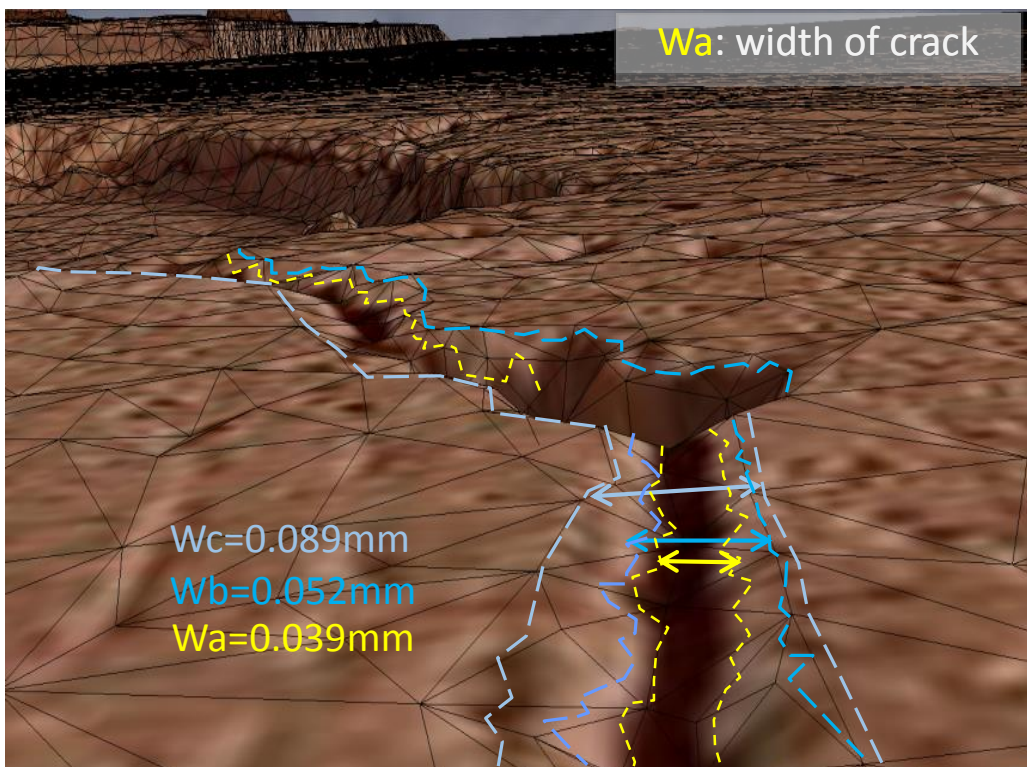


Fig. 14 Concrete wall (3D model + TIN mesh)

Table 2 Electromagnetic wave radar parameters

item	content
Frequency	1GHz
Survey mode	Time measurement, distance measurement
Thickness of rebar detection	5~300mm
Cover resolution	Range shallow : Approximately 1mm deep : Approximately 2mm
Horizontal direction resolution	Depth under 75mm : over 75mm Depth over 75mm : depth over
weight	Approximately 1kg (including battery)



$$|Ew| = \zeta \cdot |Ew_0| \cdot \exp \left[-\{\xi_t \cdot \kappa_w \cdot \sigma_{c+anion}\} \cdot \sqrt{\frac{\mu_r \mu_0}{\epsilon_r \epsilon_0} \cdot \frac{z}{2}} \right]$$

(8)

where

$|Ew|$: Output amplitude value

$|Ew_0|$: Input amplitude value

ζ : Synthetic factor of penetration and scattering

ξ_t : Conductivity correction factor from concrete temperature

κ_w : Conductivity correction factor from concrete relative humidity

$\sigma_{c+anion}$: Concrete conductivity considering chloride ion content (S/m)

μ_r : Relative permeability of concrete (= 1)

μ_0 : Permeability in the air (H/m : $4\pi \times 10^{-7}$)

ϵ_r : Relative permeability of concrete

ϵ_0 : permittivity in the air (F/m : $8.85418782 \times 10^{-12}$)

Fig. 15 Basic equation of SAE (Simulation of Attenuation Electromagnetic waves)

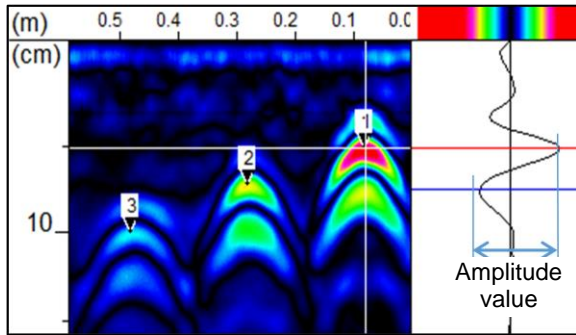


Fig. 16 Amplitude value of electromagnetic wave radar

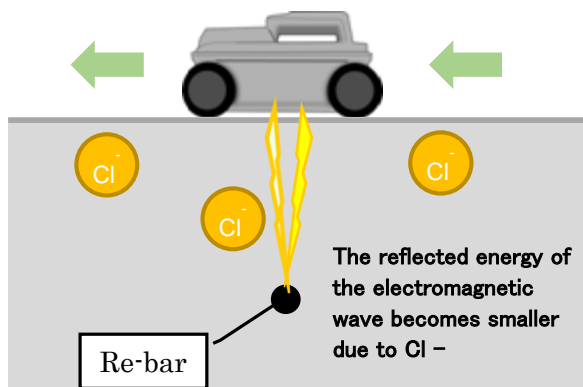


Fig. 17 Method of amplitude value acquisition with SAE

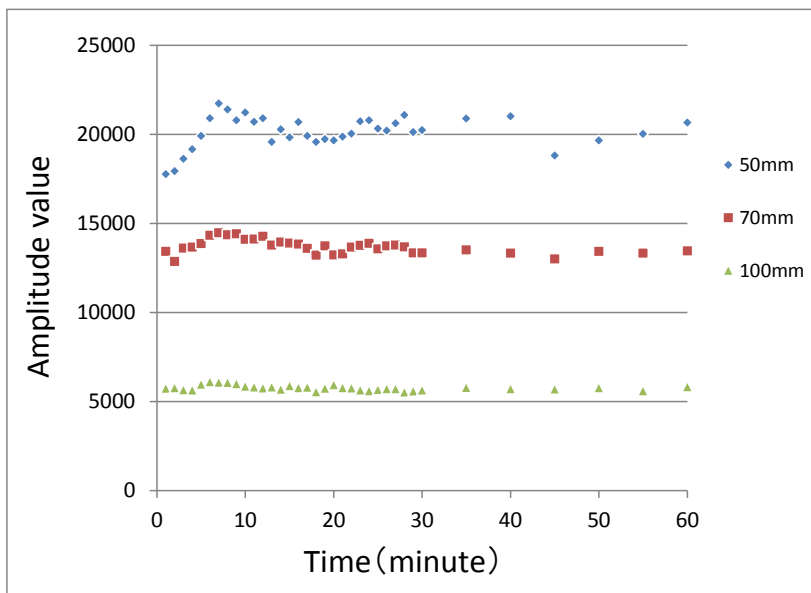
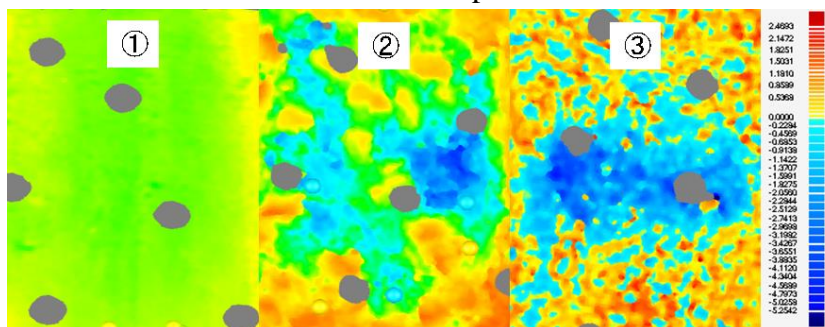


Fig. 18 Comparison of variations in power supply measurement



Surface condition of specimens



Results of measurement by 3D scanner

Fig. 19 Concrete surface roughness and 3D scanning measurement results

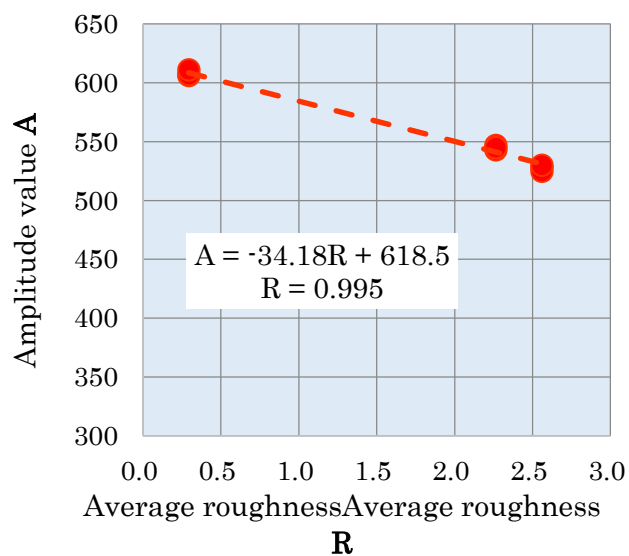


Fig. 20 Results of indoor test (surface roughness)

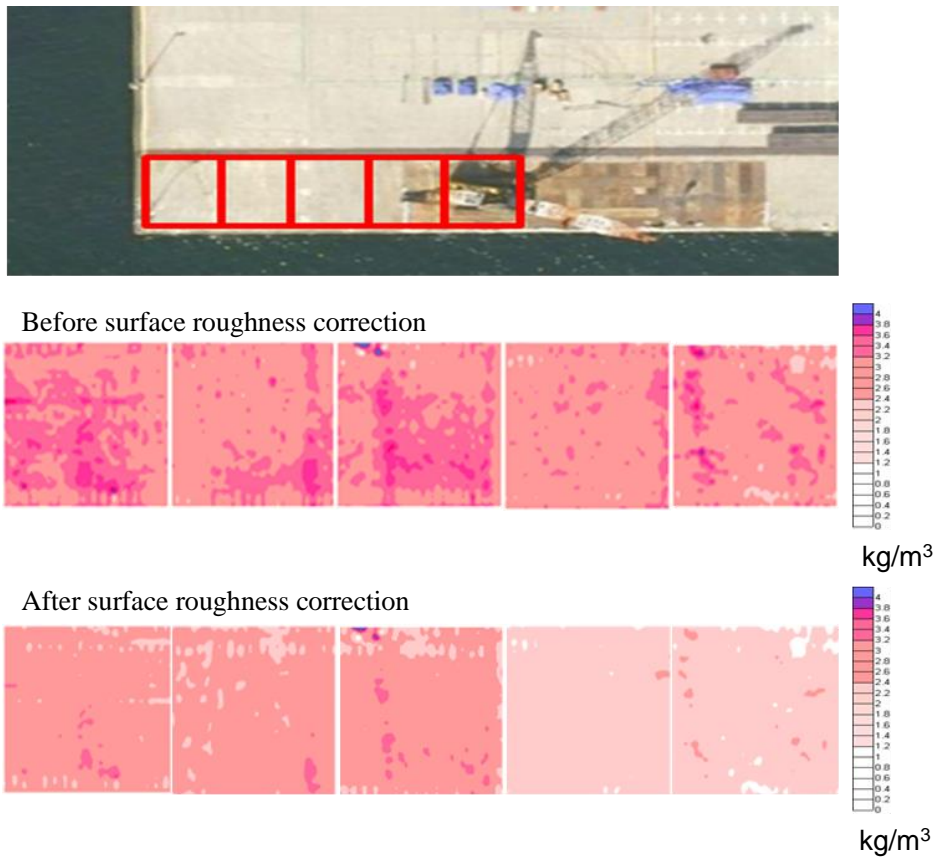


Fig. 21 Comparison of chloride ion content maps before and after surface roughness correction

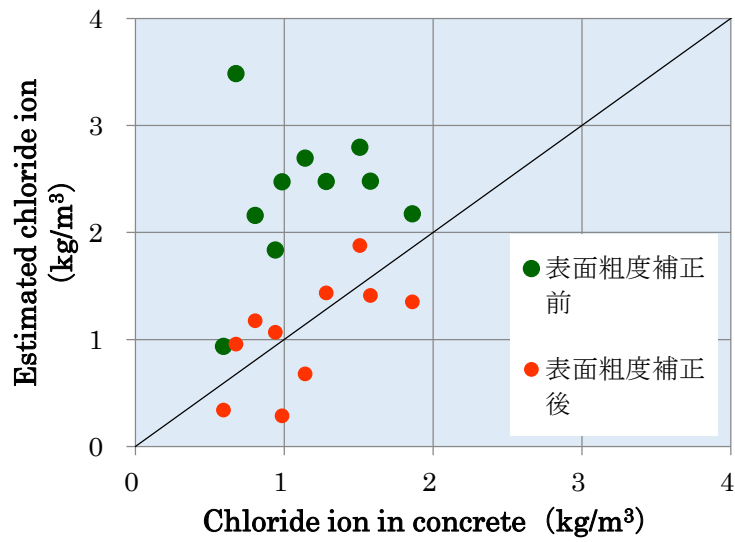


Fig. 22 Difference between values estimated by surface roughness correction and measured values

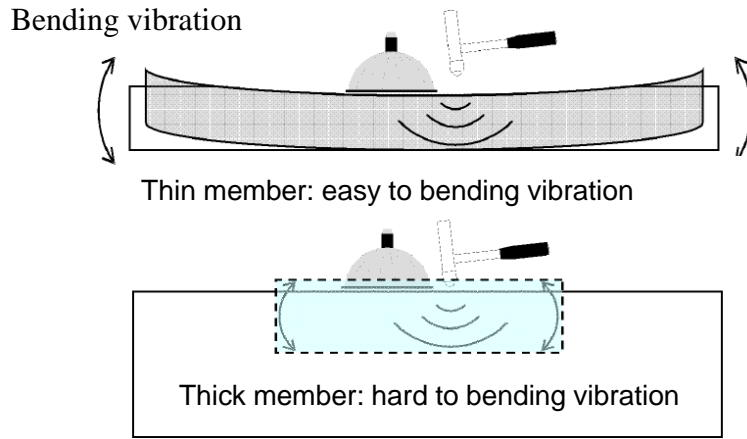


Fig.23 Bending vibration theory

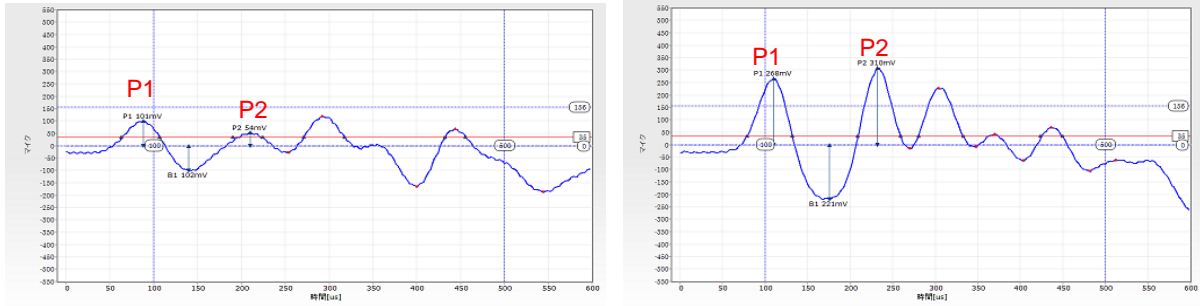


Fig. 24 Reflected sound waveform of ALP hammering device (X axis: Time (μ s), Y axis: Recorded sound (mV))

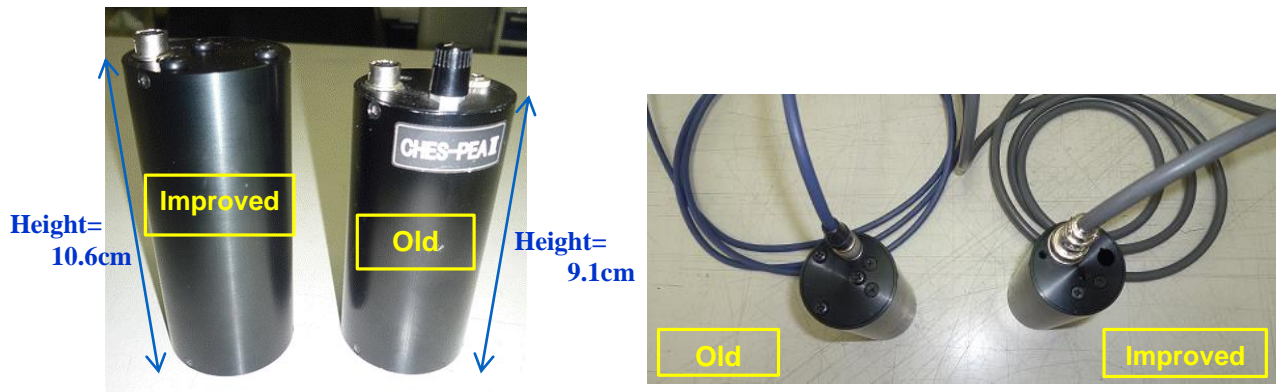


Fig. 25 Comparison of old and improved hammering devices



Fig. 26 Overview of improved striking element

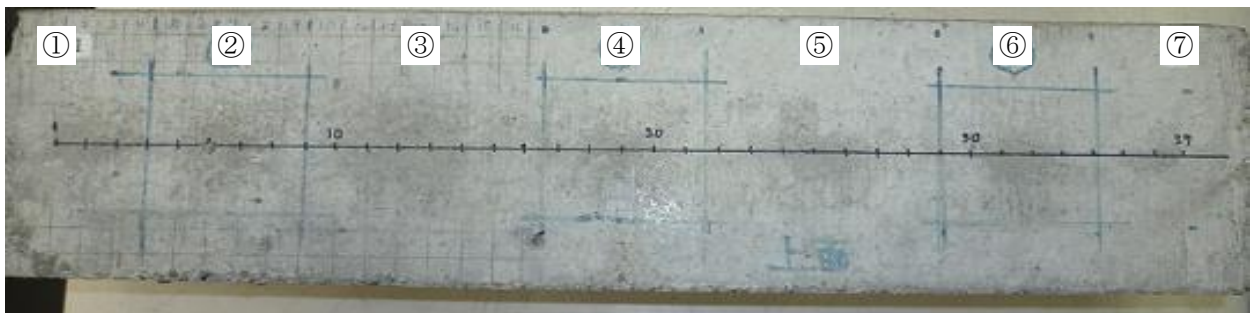


Fig. 27 Test specimen for hammering device evaluation

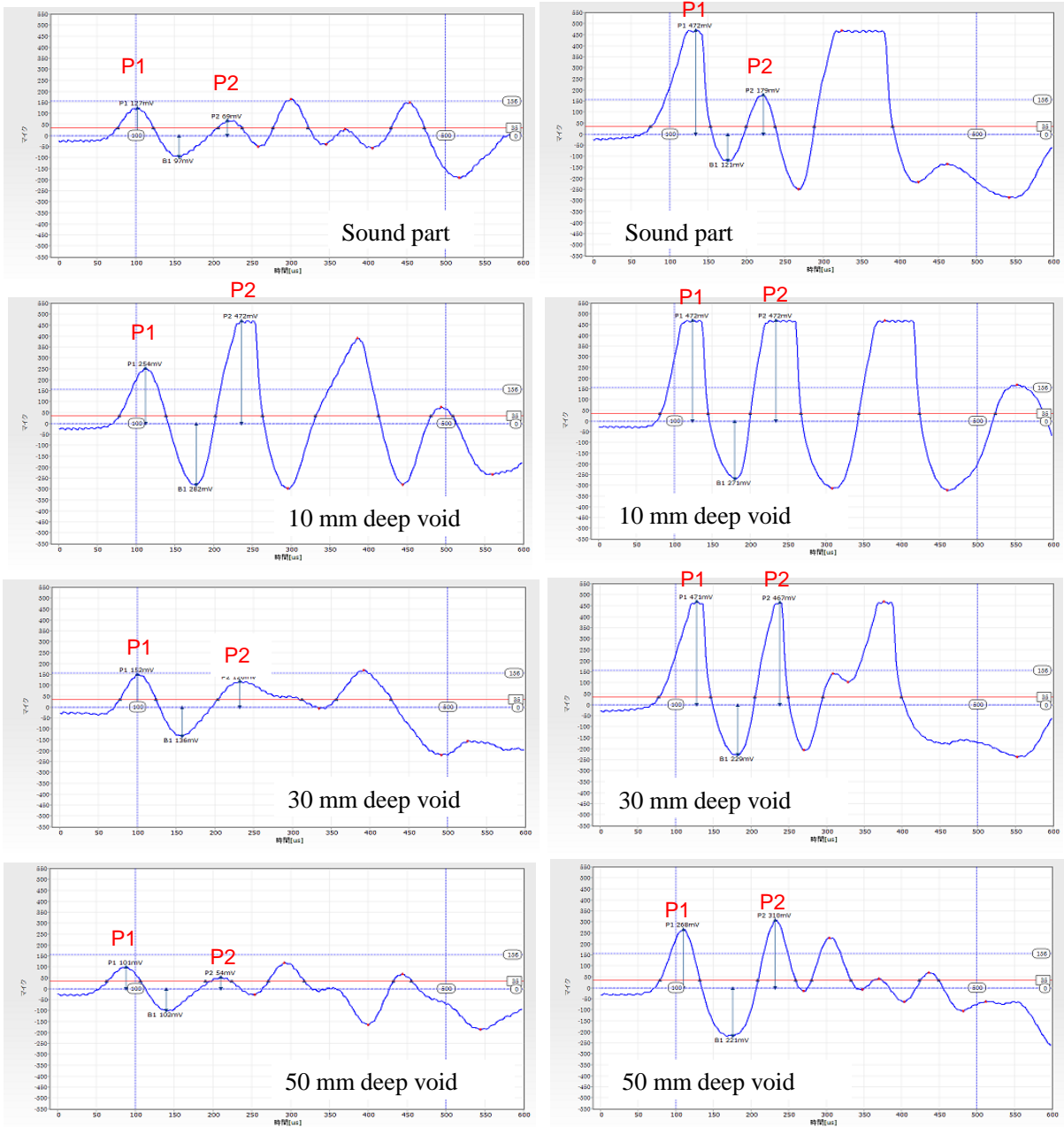


Fig. 28 Reflected sound waveform of case 1 (left) and case 4 (right) (X axis: Time (μ s), Y axis: Recorded sound (mV))

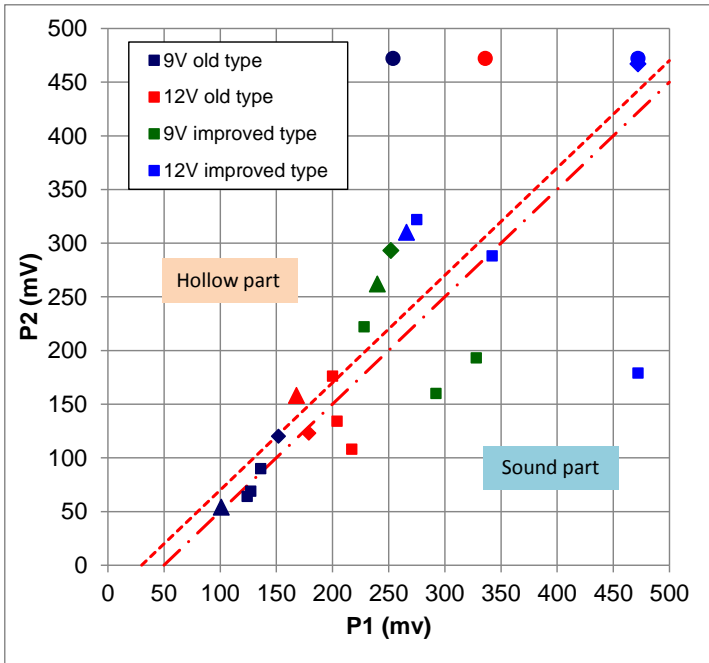


Fig. 29 Relationship between measurement results and void judgment



Fig. 30 N2U-BRIDGE (New Bridge) facility



Fig. 31 Measurement situation (specimen [1])

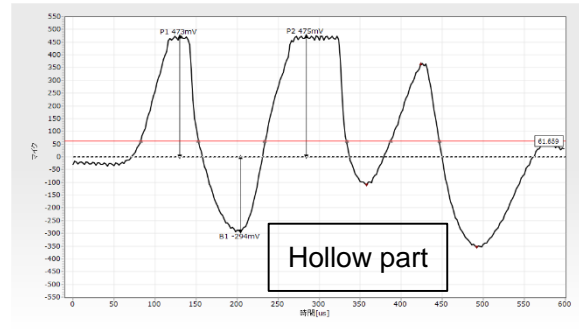
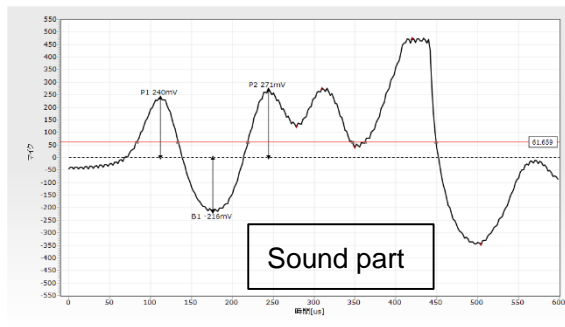


Fig. 32 Verification results of sound part and hollow part (specimen [1])



Fig. 33 Measurement situation (specimen [2])

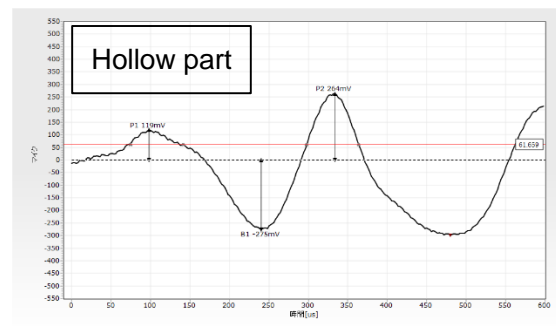
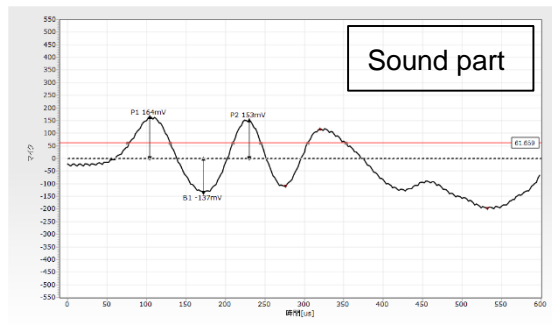


Fig. 34 Verification results of sound part and hollow part (specimen [2])



Fig. 35 Measurement situation (specimen [3])

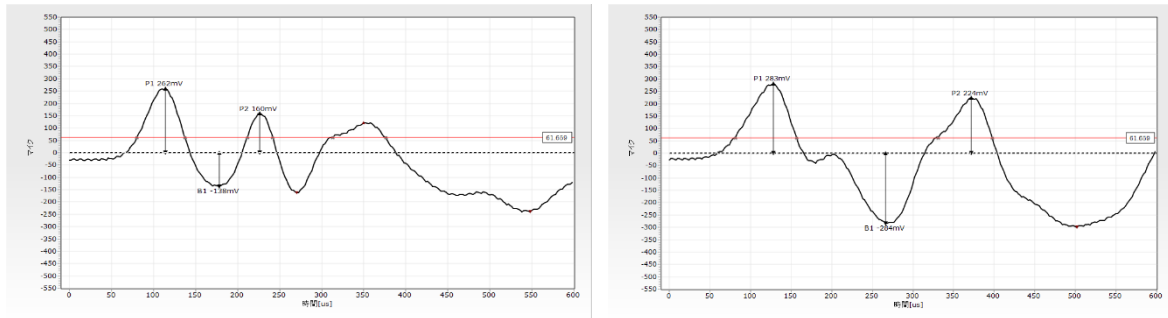
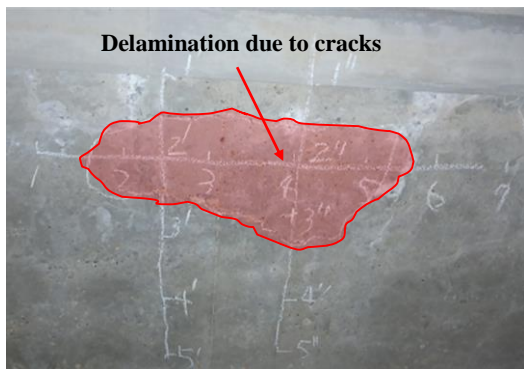


Fig. 36 Verification results of sound part and cracked part (specimen [3])



Fig. 37 Measurement situation (specimen [4])



(mV)

		1'			1''			
		16			-43			
1	2	2'	3	4	2''	5	6	7
91	473	473	473	168	219	472	204	38
		3'			3''			
		87			472			
		4'			4''			
		150			473			
		5'			5''			
		148			217			

Under 150: green, 151-250: Yellow green, over 250: red

Fig. 38 Numerical values indicating state of delamination

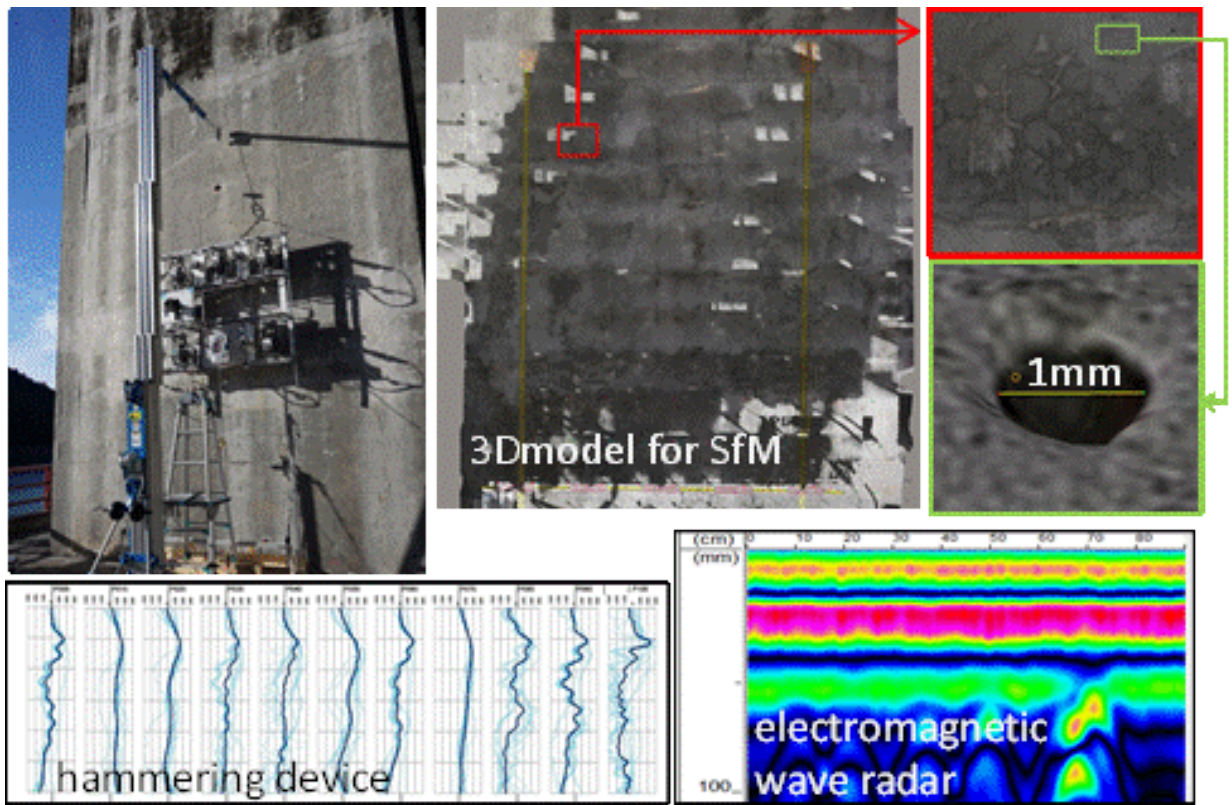
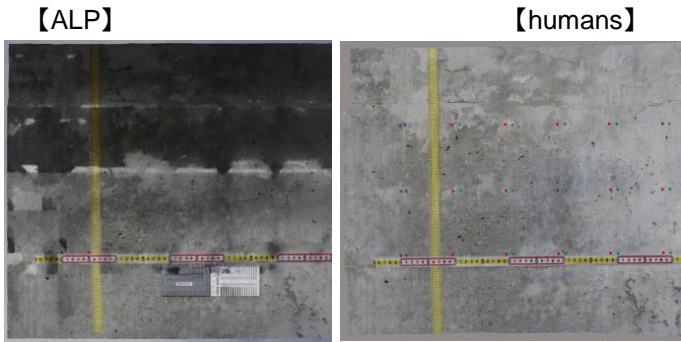
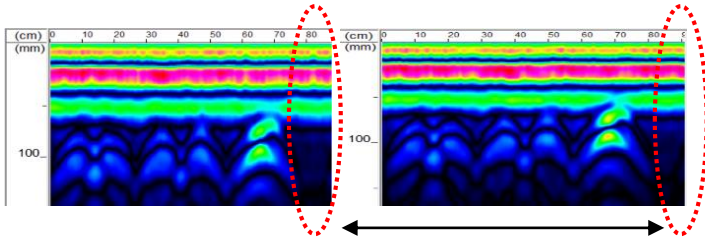


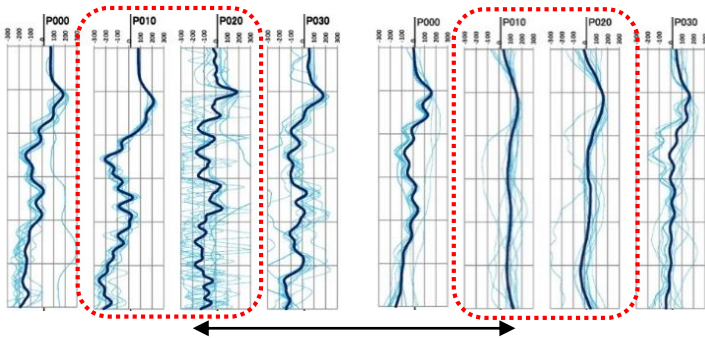
Fig. 39 ALP mounted measuring instruments



ALP is easy for shadows to appear



ALP has a slight difference in distance



ALP varies greatly

Fig. 40 Comparison of data acquired by ALP and data acquired by humans



Fig. 41 3D model created from images obtained by close inspection by ALP (approx. 30 minutes)

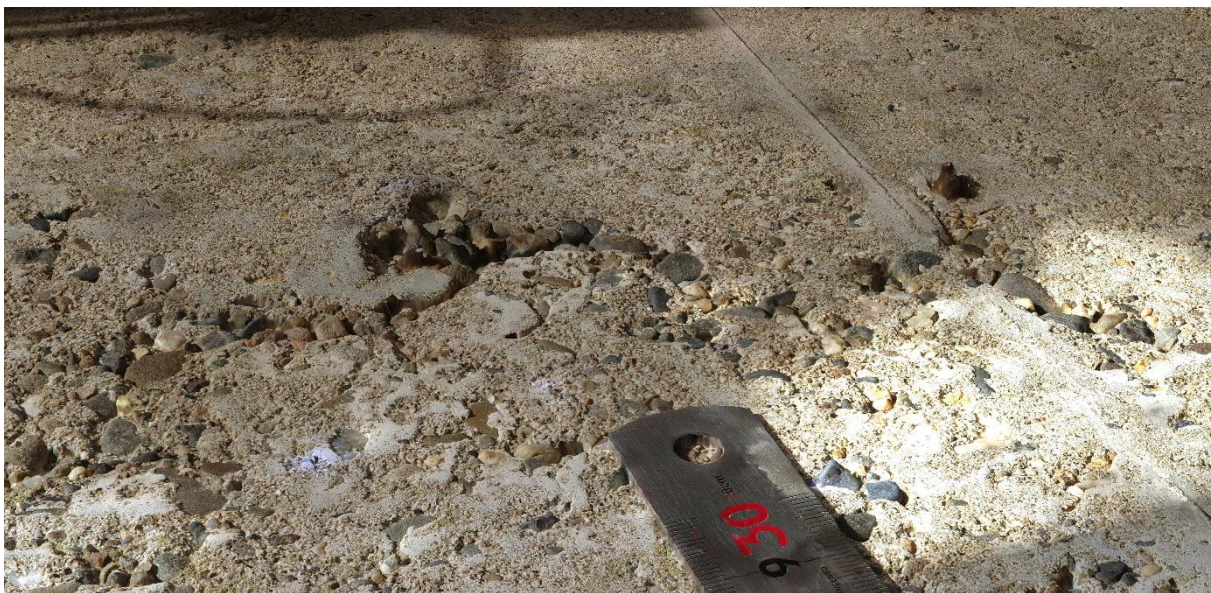


Fig. 42 Expanded view of 3D model from bird's-eye perspective